

1. Report No. NASA TN D-8025	2. Government Accession No.	3. Recipient's Catalog No.
4. Title and Subtitle TURBULENT WALL JET IN A COFLOWING STREAM		5. Report Date November 1975
		6. Performing Organization Code
7. Author(s) James F. Campbell		8. Performing Organization Report No. L-10260
9. Performing Organization Name and Address NASA Langley Research Center Hampton, Va. 23665		10. Work Unit No. 505-06-11-05
		11. Contract or Grant No.
2. Sponsoring Agency Name and Address National Aeronautics and Space Administration Washington, D.C. 20546		13. Type of Report and Period Covered Technical Note
		14. Sponsoring Agency Code
5. Supplementary Notes		
6. Abstract <p>A theoretical investigation has been undertaken to develop a relatively simple model of a two-dimensional, turbulent wall jet in a coflowing stream. The incompressible jet flow was modeled by using an integral method which includes turbulent shear stress, entrainment, and heat transfer. The method solves the conservation equations for the average jet flow properties and uses the velocity profile suggested by Escudier and Nicoll to obtain detailed characteristics of the jet on a flat plate. The analytical results compare favorably with experimental data for a range of injection velocities, which demonstrates the usefulness of the theory for estimating jet growth, velocity decay, and wall skin friction.</p> <p>The theory, which was applied to a Coanda jet on a circular cylinder, provided estimates of suction pressures aft of the jet exit that were in close agreement with experimental values.</p>		
17. Key Words (Suggested by Author(s)) Wall jet Turbulent flow	18. Distribution Statement Unclassified - Unlimited Subject Category 34	

TURBULENT WALL JET IN A COFLOWING STREAM

James F. Campbell
Langley Research Center

SUMMARY

A theoretical investigation has been undertaken to develop a relatively simple model of a two-dimensional, turbulent wall jet in a coflowing stream. The incompressible jet flow was modeled by using an integral method which includes turbulent shear stress, entrainment, and heat transfer. The method solves the conservation equations for the average jet flow properties and uses the velocity profile suggested by Escudier and Nicoll to obtain detailed characteristics of the jet on a flat plate. The analytical results compare favorably with experimental data for a range of injection velocities, which demonstrates the usefulness of the theory for estimating jet growth, velocity decay, and wall skin friction.

The theory, which was applied to a Coanda jet on a circular cylinder, provided estimates of suction pressures aft of the jet exit that were in close agreement with experimental values.

INTRODUCTION

Wall jets, have been studied for some time with principal applications to boundary-layer control and film-cooling technology (refs. 1 to 9). Another application occurs on airplanes (refs. 10 to 12) where the jet engines exhaust over the upper surfaces of the wings and interact with the wing flow field in the fashion of a wall jet (ref. 13). As pointed out by Wimpres (ref. 10), this arrangement can result in scrubbing drag which has significant effects on cruise efficiency.

The theoretical representation of a wall jet usually assumes similarity conditions of some sort in order to obtain solutions to the governing equations of fluid motion (ref. 5, for example). This limits their applicability to that region of the jet flow that is fully developed, that is, downstream of the potential-core region of the jet. Since the upper-surface-blowing wall jet can have a potential core existing to or beyond the wing trailing edge, it is desirable to have a theory that uses the jet exhaust conditions to obtain estimates of the wall-jet development from the jet exit.

Accordingly, the present study was conducted to develop a relatively simple theoretical model of a two-dimensional, turbulent wall jet in a coflowing stream, where the

two streams are parallel and flowing in the same direction. The interaction process was modeled with an integral method which includes turbulent shear stress, entrainment, and heat transfer. The method utilizes the skin-friction and entrainment equations postulated by Escudier and Nicoll (ref. 4) and solves the fluid-flow conservation equations to obtain the average jet flow properties. This technique allows the solution procedure to be the same in all regions of the developing wall jet. To estimate detailed flow characteristics, the shape of the velocity profile suggested by Escudier and Nicoll (ref. 4) was used.

This paper presents the development of this theory and shows comparisons with other theoretical methods and experimental data.

SYMBOLS

A	jet cross-sectional area
A_{av}	average jet cross-sectional area (see eq. (19))
C_p	pressure coefficient, $\frac{p_4 - p_\infty}{\frac{1}{2} \rho_\infty V_\infty^2}$
c_f	local skin-friction coefficient, $\frac{\tau}{\frac{1}{2} \rho_\infty V_\infty^2}$
c_p	specific heat at constant pressure
E	entrainment per unit length of jet in x-direction
\vec{e}_n	unit vector perpendicular to control-volume surfaces
h	jet height
K_1, K_2	boundary-layer constants (see eqs. (7) and (8))
L	parameter defined by equation (8)
m	mass in control volume
m_e	mass entrained through outer edge of control volume
p	static pressure
p_1, p_2, p_3, p_4	average static pressures on control-volume surface

1	R_h	Reynolds number based on h , $\frac{\rho_\infty V_\infty h}{\mu_\infty}$
2		
3	r	radius of curvature
4		
5	S	surface area
6		
7	s	$= \frac{1}{2} c_f$
8		
9	T	average jet temperature
10		
11	T_∞	free-stream temperature
12		
13	V	velocity
14		
15	\vec{V}	velocity vector
16		
17	V_{av}	average jet velocity in control volume
18		
19	$V_{e,x}, V_{e,y}$	velocity of outer flow at edge of jet in x- and y-direction, respectively
20		
21	V_j	average velocity over jet cross section, $\frac{1}{A} \iint V_l dA$
22		
23	V_l	velocity at point in flow
24		
25	V_{max}	maximum jet velocity
26		
27	X, Y	axes tangent and perpendicular to wall
28		
29	x, y	distances along X- and Y-axes
30		
31	Δx	length of control volume
32		
33	y_1	vertical location of V_{max} from wall surface
34		
35	y_2	vertical location where velocity excess is one-half of maximum excess (see eq. (15))
36		
37		
38	z	$= \frac{V_l}{V_{e,x}}$
39		

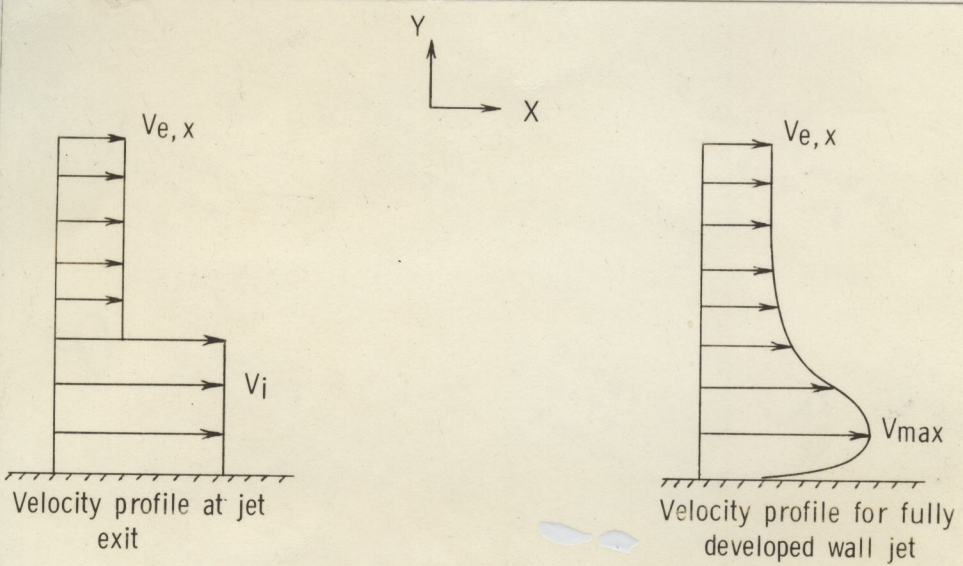
1	z_E	velocity parameter used to define velocity profile (see eq. (9))
2		
3	Γ	circulation
4		
5	$\hat{\Gamma}$	circulation parameter defined in equation (26)
6		
7	η, η_1	y/h and y_1/h , respectively
8		
9	θ	angular coordinate on cylinder (see sketch (d))
10		
11	μ	molecular viscosity
12		
13	ρ	average jet density
14		
15	ρ_l	density at a point in flow
16		
17	ρ_∞	free-stream density
18		
19	τ	average wall shear stress acting on Δx

Subscripts:

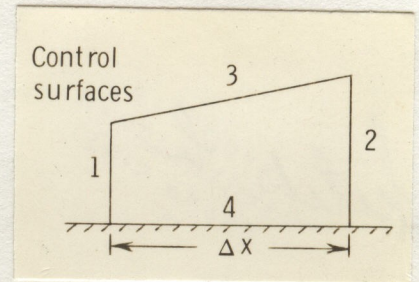
22		
23	i	condition at jet exit
24		
25	∞	free stream

THEORETICAL DEVELOPMENT

This section is concerned with the development of a theory which approximates the fluid mechanical processes that occur when a jet is injected along a wall parallel to an external, coflowing stream. This flow situation is illustrated in sketch (a) where the picture on the left shows the velocity profile at the jet exit and the picture on the right represents the velocity profile for a fully developed wall jet, which occurs at some distance downstream of the exit. The present development examines the class of jet flows where the injection velocity V_i is greater than the velocity $V_{e,x}$ of the adjacent flow. For a wall jet on a flat plate with no streamwise pressure gradient, $V_{e,x}$ is equivalent to the free-stream velocity V_∞ .



Sketch (a)



Sketch (b)

The integral form of the Navier-Stokes equations for the conservation of mass and momentum is applied to a section of the jet flow which is considered as a control volume. (See sketch (b).)

Conservation of Mass

Equation 6.11 of reference 14 provides the integral expression for conservation of mass, which equates the net influx of mass into the control volume to the rate of increase of mass in the control volume. It is assumed that the flow process is steady (in the mean) so that the continuity equation can be written as

$$\oint_S \rho_l \vec{v} \cdot \vec{e}_n dS = 0 \quad (1)$$

where

$dS \equiv$ Elemental surface area

and

$\vec{e}_n \equiv$ Unit vector perpendicular to control surfaces

Carrying out the operations suggested by equation (1) leads to the mass flows through surfaces 1, 2, and 3. Since mass flow is a single-valued function of position along the wall, a Taylor expansion can be performed to obtain mass flow through surface 2 as a

function of the mass flow through surface 1. The difference between the mass flows through surfaces 1 and 2 represents the entrainment of fluid across surface 3, which is written as

$$E = \frac{d}{dx} \left(\iint \rho_l V_l dA \right) = \frac{d(\rho A V_j)}{dx} \quad (2)$$

where E is the entrainment per unit length of the jet in the x -direction. For a two-dimensional flow,

$$E = \frac{d}{dx} \left(\int \rho_l V_l dy \right) \quad (3)$$

In the present formulation, the entrainment law recommended by Escudier and Nicoll (ref. 4) for wall jets on flat plates is used to specify E . This is given as

$$\frac{E}{\rho_\infty V_\infty} = 0.03 z_E - 0.02 \quad (4)$$

where z_E is used in reference 4 to relate entrainment levels to jet flow properties. The parameter z_E represents the ratio of the law-of-the-wall velocity at the outer edge of the boundary layer to the mainstream velocity and is defined in a later section. For wall jet flows $z_E > 1$. Experimental entrainment rates from reference 4 are presented in figure 1 as a function of z_E and were obtained for incompressible flows for a range of V_i/V_∞ from about 2 to 20. As can be seen, the experimental values compare reasonably well with the values estimated by equation (4).

Conservation of Momentum

The integral expression for the conservation of momentum is obtained from equation 6.12 of reference 14, which shows that the rate of increase of momentum in the control volume is equal to the sum of forces acting on the control volume plus the net influx of momentum into the control volume. Since equation 6.12 of reference 14 was developed for a nonviscous flow process, another term has to be added to that equation to account for the shear stress on the control-volume surfaces. The forces due to shear stress are in addition to the pressure and body forces already present in the governing equation.

The flow process is taken to be independent of time, similar to the assumption for mass conservation.

x -direction. - The integral equation is applied to the control volume to obtain the momentum flux in the x -direction. It is assumed that the shear stress is zero at the interface between the jet and external flow since $V_l = V_{e,x}$. Hence, the shear stress at the wall is the only shear stress acting on the control-volume surfaces. Taking the body

force in the x-direction to be zero results in a momentum equation similar to equations (26.34) and (27.18) in reference 15, which were derived for application to a boundary layer. After assuming average density and velocity over the jet cross section, the x-momentum equation can be written in differential form as

$$\frac{d(\rho AV_j^2)}{dx} = -h \frac{dp}{dx} - \tau + V_{e,x} E \quad (5)$$

For the application of this equation to a flat plate, the term dp/dx is assumed to be zero, and $V_{e,x} = V_\infty$.

y-direction. - The integral equation from reference 14 (eq. 6.12) is applied to the control volume to obtain the y-momentum equation, which is needed to solve for the development of a wall jet on a curved surface. It is assumed that the jet flow adheres to the curved surface, a phenomenon which is usually referred to as a Coanda jet. A body force is present in the form of a centrifugal force, which results when a mass follows a curved path. The derivation yields the following momentum equation:

$$\frac{\rho AV_j^2}{r} = (p_3 - p_4) + V_{e,y} E \quad (6)$$

where r is the radius of curvature and p_3 and p_4 are average static pressures at the outside edge of the jet and at the wall, respectively. The normal velocity at the edge of the jet $V_{e,y}$ is defined in terms of entrainment as

$$V_{e,y} = E/\rho$$

which is similar to the definition used in reference 4. It should be noted that Levinsky and Yeh developed an integral theory for a turbulent Coanda jet but did not include the entrainment term (last term on the right side of eq. (6)) in their normal momentum equation. (See eq. (20) in ref. 16.)

Skin Friction

Following reference 4, the velocity profile at the edge of the flow gives the following skin-friction law:

$$s \equiv \frac{1}{2} c_f = \frac{\tau}{\rho_\infty V_\infty^2} = \left(\frac{K_1 z E}{L} \right)^2 \quad (7)$$

where

$$L = \ln \left(K_2 R_h s^{1/2} \right) \quad (8)$$

The constants K_1 and K_2 are specified in reference 4 to be 0.40 and 6.542, respectively, for wall jets on flat plates. These values are used for all the calculations presented in this paper.

Velocity Profile

Now that the entrainment and shear stress laws have been appropriately defined, equation (5) can be solved for the jet momentum, which in turn can yield the average jet velocity. At this point it is useful to specify the form of the velocity profile for the wall jet in order to check the solution against available data, which are usually presented in terms of velocity profile parameters. In addition, the specified profile provides z_E in the expressions for E and τ (eqs. (4) and (7), respectively).

The velocity profile used herein is that of Escudier and Nicoll (ref. 4) for flat-plate flows and is a two-component profile which is built up by superposition of a wake component and a logarithmic law-of-the-wall component. (See fig. 2.) These components are combined to give the total velocity profile as follows:

$$z = \frac{V_L}{V_{e,x}} = z_E \left(1 + \frac{\ln \eta}{L} \right) + \frac{1}{2} (1 - z_E) (1 - \cos \pi \eta) \quad (9)$$

where the first term on the right side of the equation represents the logarithmic law-of-the-wall component and the second term represents the wake component. It is noted that $z = 1$ at $\eta = 1$ and that $z \rightarrow -\infty$ very close to the wall where $\eta \rightarrow 0$. Although $V_L \rightarrow -\infty$ at the wall, this does not present a problem in the way the velocity profiles are used in the present study.

To relate the velocity profile parameters in equation (9) to the theoretical solution for the average velocity, the definition

$$V_j = \frac{\int_0^h V_L dy}{\int_0^h dy} = V_{e,x} \int_0^1 \frac{V_L}{V_{e,x}} d\eta \quad (10)$$

is used. Substituting for $V_L/V_{e,x}$ from equation (9) into equation (10) and performing the integration yields

$$\frac{V_j}{V_{e,x}} = z_E \left(\frac{1}{2} - \frac{1}{L} \right) + \frac{1}{2} \quad (11)$$

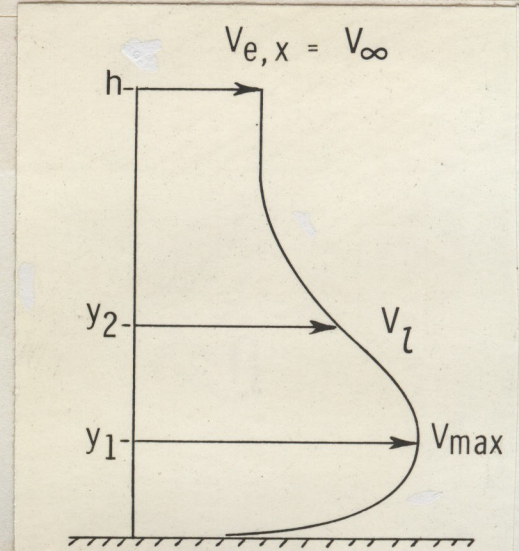
This is rearranged into a more suitable form to get

This is rearranged into a more suitable form to get

$$z_E = \left(\frac{2L}{L-2} \right) \frac{V_j}{V_{e,x}} - \left(\frac{L}{L-2} \right) \quad (12)$$

where it is noted that z_E is a linear function of $V_j/V_{e,x}$ with the slope and intercept being functions of L .

Sketch (c) shows two of the most important parameters associated with the wall-jet velocity profile; these are the maximum jet velocity V_{max} and the location y_2 where the velocity excess $(V_l - V_\infty)$ is one-half of the maximum velocity excess $(V_{max} - V_\infty)$. This definition for y_2 allows a measure of jet growth. The maximum jet velocity obtained from equation (9) is



Sketch (c)

$$z_1 = z_E \left(1 + \frac{\ln \eta_1}{L} \right) + \frac{1}{2} (1 - z_E) (1 - \cos \pi \eta_1) \quad (13)$$

where η_1 is obtained by differentiating equation (9) with respect to η , setting $dz/d\eta = 0$, and then solving the remaining equation for η_1 . To perform this final step, a series expansion of $\sin(\pi \eta_1)$ is necessary. Reference 4 showed that the values for η_1 range between 0.1 and 0.2, which means that $\pi \eta_1 < 1$, so that most of the expansion terms can be ignored. If the first and second terms (i.e., η_1 and η_1^3) are retained, a quartic equation for η_1 is obtained. Investigation showed that the solution for this quartic equation gave essentially the same answer that was obtained by retaining only the first expansion term and solving the resulting quadratic equation. Hence, the latter procedure was adopted and yielded the following expression for η_1 :

$$\eta_1 = \left[\frac{2z_E}{\pi^2 L (1 - z_E)} \right]^{1/2} \quad (14)$$

The jet height y_2 is defined as the value of y where

$$V_l - V_{e,x} = \frac{1}{2} (V_{max} - V_{e,x}) \quad (15)$$

This equation can be written in terms of z_1 :

$$\frac{V_L}{V_{e,x}} = \frac{1}{2}(z_1 + 1) \quad (16)$$

Thus, if z_1 is known from equation (13), then equation (16) yields the velocity corresponding to y_2 . A linear interpolation procedure was used with equation (9) to determine the velocity specified by equation (16), which thus yielded y_2 .

Heat Content

The average temperature of the jet can be determined by accounting for the change in heat content per unit volume ($\rho c_p T$) of the jet flow due to the entrainment of free-stream flow at a different energy level $(\rho c_p T)_\infty$. Applying this concept to the control volume results in the expression

$$(m c_p T)_{n+1} = (m c_p T)_n + m_e (c_p T)_\infty \quad (17)$$

where $(m c_p T)_n$ represents the energy level that would exist in the control volume at point n if there were no entrainment, and $(m c_p T)_{n+1}$ represents the equilibrium energy level at point $n+1$ resulting from the complete mixing of the jet and entrained flows. The various specific heats in equation (17) are assumed to have the same value.

The mass in the control volume before entrainment m_n is approximated by

$$m_n = \rho_n A_{av} \Delta x \quad (18)$$

where

$$A_{av} = \frac{A_n + A_{n+1}}{2} \quad (19)$$

The mass entrained through the outer edge of a control volume with length Δx is given by

$$m_e = \frac{\Delta x (\rho A V_j)_e}{V_{av}} \quad (20)$$

where

$$V_{av} = \frac{V_{j,n+1} + V_{j,n}}{2} \quad (21)$$

Since

$$(\rho AV_j)_e = \Delta x \frac{d(\rho AV_j)}{dx} = \Delta x E \quad (22)$$

equation (20) can be written as

$$m_e = \frac{(\Delta x)^2 E}{V_{av}} \quad (23)$$

The mass in the control volume after entrainment takes place is

$$m_{n+1} = m_n + m_e \quad (24)$$

By knowing the values for T_∞ and T_n , equation (17) can be solved for T_{n+1} , which can then be used to calculate the jet density and viscosity properties by using the equation of state and Sutherland's formula, respectively. In the current paper, jet temperatures were calculated only for wall jets with no pressure gradients (i.e., flat-plate flows); therefore, the pressure value used in the equation of state was assumed to be ambient.

Application to a Cylinder

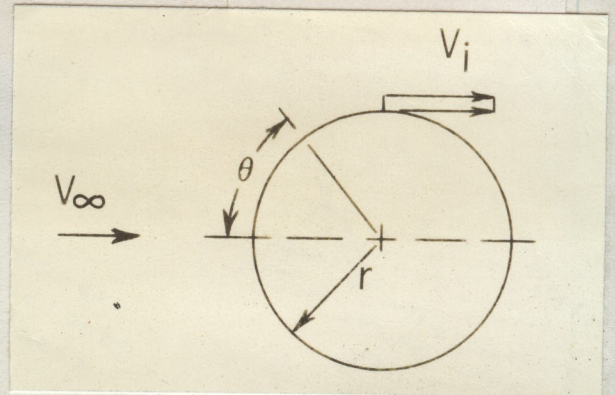
The solution capability of the present theory for calculating wall-jet development on curved surfaces is illustrated here by looking at a circular cylinder with a thin wall jet.

In particular, the example consists of a cylinder with tangential blowing at the shoulder which was investigated in reference 16 and is illustrated in sketch (d). To solve the governing equations for a wall jet on the cylinder, it is necessary to provide the flow conditions at the edge of the jet flow. Following Levinsky and Yeh, this is accomplished by using potential flow velocities and pressures on a cylinder with circulation, where the coflowing velocity at the jet boundary, which is needed in the x-momentum equation (eq. (5)), is given by

$$V_{e,x} = 2V_\infty (\sin \theta + \hat{\Gamma}) \quad (25)$$

where

$$\hat{\Gamma} = \frac{\Gamma}{4\pi r V_\infty} \quad (26)$$



Sketch (d)

The pressure at the edge of the jet can be obtained from equation (25) and Bernoulli's equation. Thus,

$$\frac{p_3 - p_\infty}{\frac{1}{2} \rho_\infty V_\infty^2} = 1 - 4(\sin \theta + \hat{\Gamma})^2 \quad (27)$$

which provides p_3 in the normal momentum equation (eq. (6)). The pressure gradient required in equation (5) is

$$\frac{dp}{dx} = -\frac{4\rho V_\infty^2}{r}(\sin \theta + \hat{\Gamma}) \cos \theta \quad (28)$$

The value of $\hat{\Gamma}$ used in these expressions (0.29) was obtained in reference 16 and resulted in the best estimate of the experimental data on the windward surface of the cylinder. To obtain a solution for the wall jet on the cylinder, it is assumed that the entrainment and shear stress laws used previously for the flat-plate problem are applicable in this situation.

Solution Procedure

A computer program was written to solve the governing equations for the average flow properties in the jet. This consisted of an iterative method which solved the equations as an initial-value problem. The sequence of calculations in the computer program is as follows:

- (1) Define properties at jet exit.
- (2) Guess values at first step away from jet exit (i.e., ρ_{n+1} , h_{n+1} , $V_{j,n+1}$, L_{n+1} , and $z_{E,n+1}$).
- (3) Calculate the following parameters prior to solving x-momentum equation:

s_{n+1} from equation (7)

$$R_h = \frac{\rho_\infty V_\infty h_{n+1}}{\mu_\infty}$$

L_{n+1} from equation (8)

$z_{E,n+1}$ from equation (12)

E_{n+1} from equation (4)

$$(\rho AV_j)_{n+1} = E_{n+1} \Delta x + (\rho AV_j)_n \quad (29)$$

(where a backward finite difference is used in eq. (2) to obtain $(\rho AV_j)_{n+1}$ in terms of E_{n+1})

s_{n+1} from equation (7) by using latest values of z_E and L

τ_{n+1} from s_{n+1} (eq. (7))

$$\left. \begin{array}{l} V_{e,x} = V_\infty \\ \frac{dp}{dx} = 0 \end{array} \right\} \text{For flat plate}$$

$$\left. \begin{array}{l} V_{e,x} \text{ from equation (25)} \\ \frac{dp}{dx} \text{ from equation (28)} \end{array} \right\} \text{For cylinder}$$

(4) Solve equation (5) for the change in x-momentum $\left. \frac{d(\rho AV_j^2)}{dx} \right|_{n+1}$ by using the current values for shear stress, pressure gradient, entrainment, and external velocity. This parameter is then approximated with a backward finite difference which allows the jet momentum to be calculated as follows:

$$(\rho AV_j^2)_{n+1} = \Delta x \left. \frac{d(\rho AV_j^2)}{dx} \right|_{n+1} + (\rho AV_j^2)_n$$

The average velocity and height follow:

$$V_{j,n+1} = \frac{(\rho AV_j^2)_{n+1}}{(\rho AV_j)_{n+1}}$$

and

$$h_{n+1} = \frac{(\rho AV_j)_{n+1}}{\rho_{n+1} V_{j,n+1}}$$

(5) Obtain the pressure increment between the outer edge of the jet and the curved wall surface ($p_3 - p_4$) by using the y-momentum expression (eq. (6)). If the wall surface is flat, then the y-momentum equation would not be solved. The pressure increment

is flat, then the y-momentum equation would not be solved. The pressure increment $(p_3 - p_4)$ is combined with equation (27) to calculate the cylinder surface pressure p_4 .

(6) Calculate T_{n+1} from equation (17), then ρ_{n+1} and μ_{n+1} .

(7) Go back to step (3) and repeat the solution procedure using the most recently calculated values for the parameters at point $n+1$. The number of iterations necessary to achieve a converged solution was examined; it appeared that four iterations were adequate.

(8) Compute the velocity profile by using the values of z_E and L obtained from the preceding solution. The actual profile is provided by equation (9), which also yields a value for y_2 through the use of equation (16). The location and magnitude of V_{\max} is obtained from equations (14) and (13), respectively.

This procedure is repeated at each incremental step along the plate to obtain the final solution. The effect of the magnitude of this step was examined and was found to be insignificant when the value of the step size was less than h_i . The step size used to calculate the results presented herein was $0.10h_i$.

RESULTS AND DISCUSSION

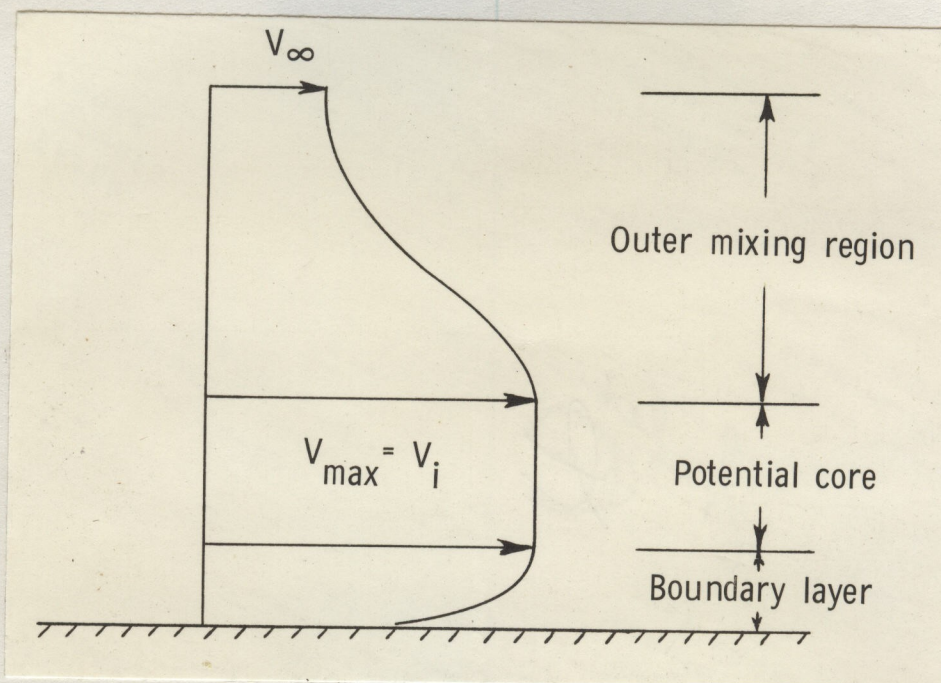
Flat Plate

Velocity profiles.- A comparison of experimental and theoretical velocity profiles is presented in figure 3 for a range of injection velocities and distances along the flat plate. For these comparisons, V_∞ is equivalent to $V_{e,x}$. The experimental data obtained by Neale (ref. 7) illustrate velocity profiles that are typical of wall jets; that is, the maximum jet velocity occurs close to the wall and decreases with increases in x/h_i . The theoretical profiles are in reasonable agreement with the experimental profiles for all of the injection velocities presented. There appears to be a tendency for the theory to slightly underpredict the maximum velocity, particularly at the higher values of V_i/V_∞ . In addition, the experimental data indicate that the vertical location where the maximum velocity occurs is a little closer to the wall than predicted by the theory.

Velocity decay and jet growth.- A comparison of experimental and theoretical results for the wall-jet development is presented in figures 4 to 9 for a range of V_i/V_∞ from 2 to 18. The graphs show the maximum jet velocity normalized by the initial jet velocity V_{\max}/V_i and a measure of jet growth normalized by the initial jet height y_2/h_i as functions of the nondimensional distance along the plate. It is noted that in reference 9, George based the injection conditions (V_i/V_∞ equals 2.80 and 5.55) on the maximum velocities at the jet exit. In figures 5 and 7, these data are referenced to the average values of V_i noted previously. Where there is more than one value of V_i/V_∞ shown in a figure, the values associated with the experiment of Neale (ref. 7) are used for the calculations.

The present theory provides generally good predictions of the velocity decay and jet growth throughout the range of values for V_i/V_∞ . At the higher values of V_i/V_∞ (10.0 and 18.2 in figs. 8 and 9, respectively) the current estimates of V_{\max} are somewhat higher than experiment. Additional estimates of the jet decay characteristics are shown in figures 6, 8, and 9. These were made with the methods developed by Escudier and Nicoll (ref. 4) and by Gartshore and Newman (ref. 6) and substantiate the results of the present theory.

One limitation of these previous theories has to do with their application to the potential core region of the jet, that is, the initial mixing region where $V_{\max} = V_i$. For example, the theory of Escudier and Nicoll requires that the starting point for the solution be in the fully developed region downstream of the potential core. In addition, the method of Gartshore and Newman neglects the potential-core region and assumes that the fully developed velocity profile exists at the jet exit. The current theory is not restricted to any particular region of the jet since the solution is for the average jet properties and therefore can begin at the jet exit and march downstream. To obtain detailed velocity profiles in the potential-core region (sketch (e)), the current theory can be used by making appropriate assumptions for the distribution of velocity in the mixing region at the outer edge of the jet and in the boundary layer adjacent to the wall. Abramovich (ref. 2, p. 477), for example, assumed a power-law profile in the boundary layer and a velocity distribution in the outer portion of the jet appropriate to the initial mixing of two parallel streams.



Sketch (e)

Skin friction. - A comparison of experimental and theoretical skin-friction coefficients is presented in figure 10 for several values of V_i/V_∞ . The experimental data are from reference 7 and show that the skin friction decreases as the distance along the plate increases. This trend is typical of a turbulent wall jet and is analogous to the development of a turbulent boundary layer. As would be expected, an increase in injection velocity results in larger values of c_f all along the plate. The present theory estimates reasonably well the decrease of c_f with an increase of x/h_i and the increase of c_f with an increase of V_i/V_∞ . As noted in the figure, two sets of calculations were made. The solid line represents estimates of c_f using the injection jet temperatures T_i that correspond to the measurements, and the dashed line represents calculations that resulted from letting T_i equal T_∞ . Using the ambient value for T_i results in slightly higher theoretical values of c_f for each value of V_i/V_∞ . The reason for showing the calculations made with $T_i = T_\infty$ was to illustrate the sensitivity of the theoretical estimates to changes in jet temperature. Also, most of the experimental data presented in the preceding figures were obtained with $T_i = T_\infty$.

Cylinder

An example of wall pressures calculated by the theory is shown in figure 11, which presents surface pressures on a cylinder where the jet exit is located at the shoulder ($\theta = 90^\circ$). The results were obtained for $V_i/V_\infty = 7.24$ and $h_i/r = 0.0057$.

As noted, the potential theory (solid line) predicts the pressures on the windward surface ($0^\circ < \theta < 90^\circ$) reasonably well but underestimates the suction pressures aft of the jet exit. The method of reference 16 provides better estimates of the suction pressures aft of the jet exit. The present theory (dashed line) provides predictions similar to those of reference 16 immediately aft of the jet exit but results in better estimates as $\theta \rightarrow 180^\circ$. However, these values are still less negative than the experimental values of C_p .

It is recalled that the estimates using the present theory were obtained with flat-plate values for entrainment and shear stress. If more appropriate values were used, the agreement in figure 11 might be improved.

CONCLUDING REMARKS

A theoretical investigation has been undertaken to develop a relatively simple model of a two-dimensional, turbulent wall jet in a coflowing stream. The incompressible flow was modeled by using an integral method which includes turbulent shear stress, entrainment, and heat transfer.

The method uses the skin-friction and entrainment laws postulated by Escudier and Nicoll and solves the fluid-flow conservation equations to obtain the average jet properties.

1 In addition, detailed jet characteristics on a flat plate were obtained by using the velocity
2 profile suggested by Escudier and Nicoll. The analytical results compare favorably with
3 experimental data for a range of injection velocities, which demonstrates the usefulness
4 of the theory for estimating jet growth, velocity decay, and wall skin friction.

5 The theory, which was applied to a Coanda jet on a circular cylinder, provided rea-
6 sonable estimates of experimental suction pressures aft of the jet exit.

7
8 Langley Research Center

9 National Aeronautics and Space Administration

10 Hampton, Va. 23665

11 July 25, 1975
12
13
14
15
16
17
18
19
20
21
22
23
24
25
26
27
28
29
30
31
32
33
34
35
36
37
38
39

16. Levinsky, E. S.; and Yeh, T. T.: Analytical and Experimental Investigation of Circulation Control by Means of a Turbulent Coanda Jet. NASA CR-2114, 1972.

2
3
4
5
6
7
8
9
10
11
12
13
14
15
16
17
18
19
20
21
22
23
24
25
26
27
28
29
30
31
32
33
34
35
36
37
38
39

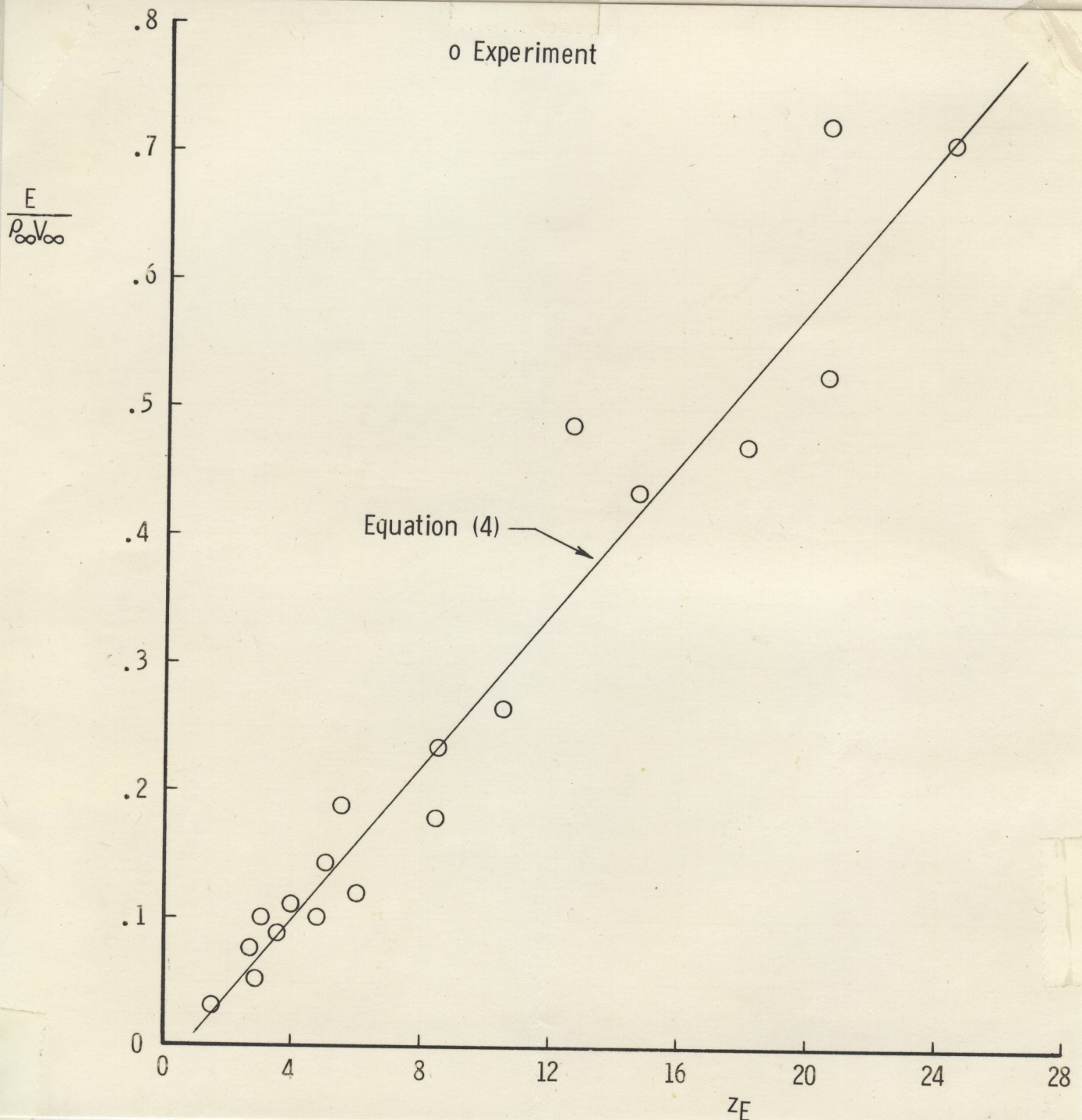


Figure 1.- Entrainment rates for two-dimensional wall jets (see ref. 4, fig. 15) with values of V_i/V_{∞} from 2 to 20.

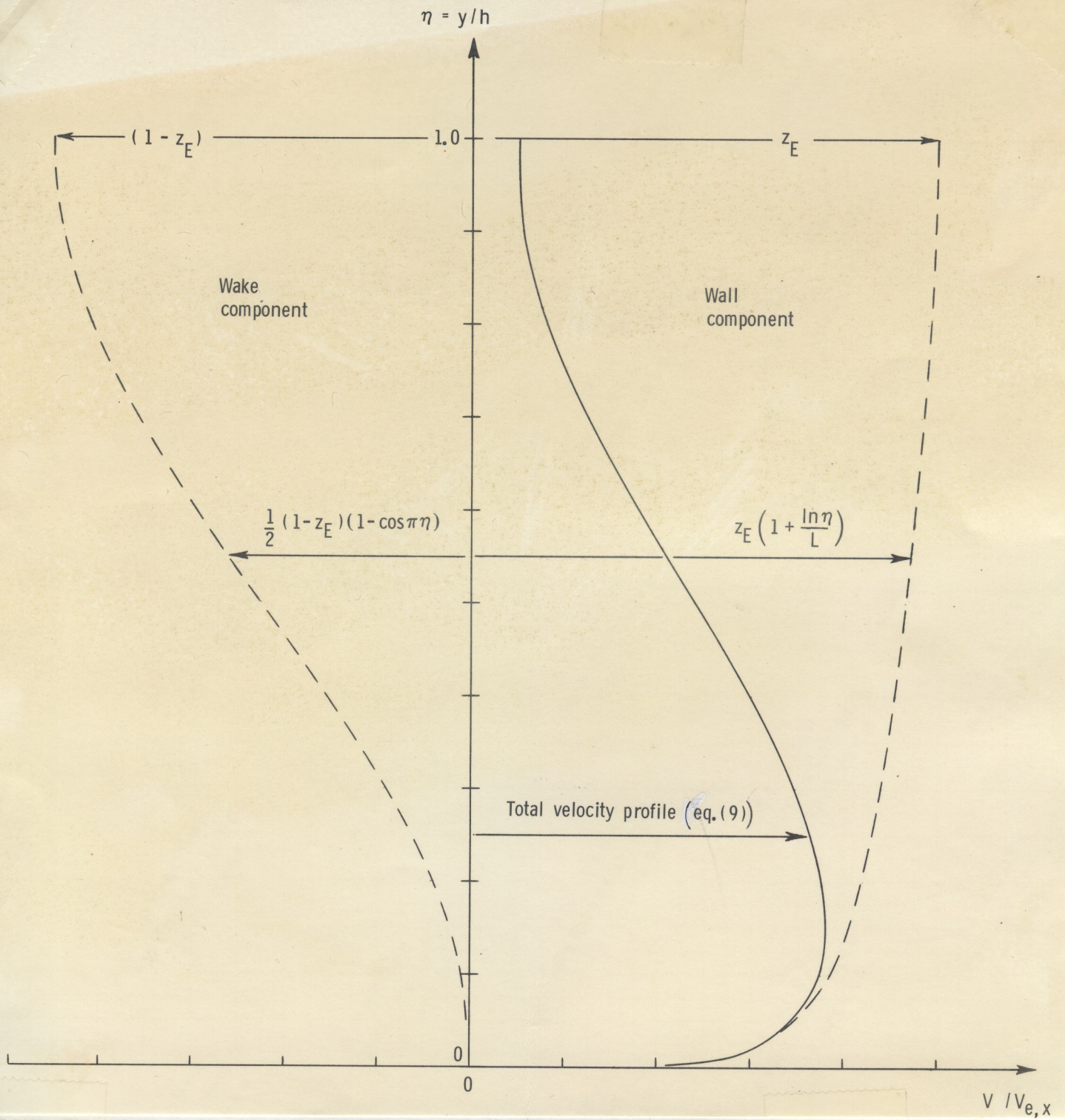


Figure 2.- Wall-jet velocity profile.

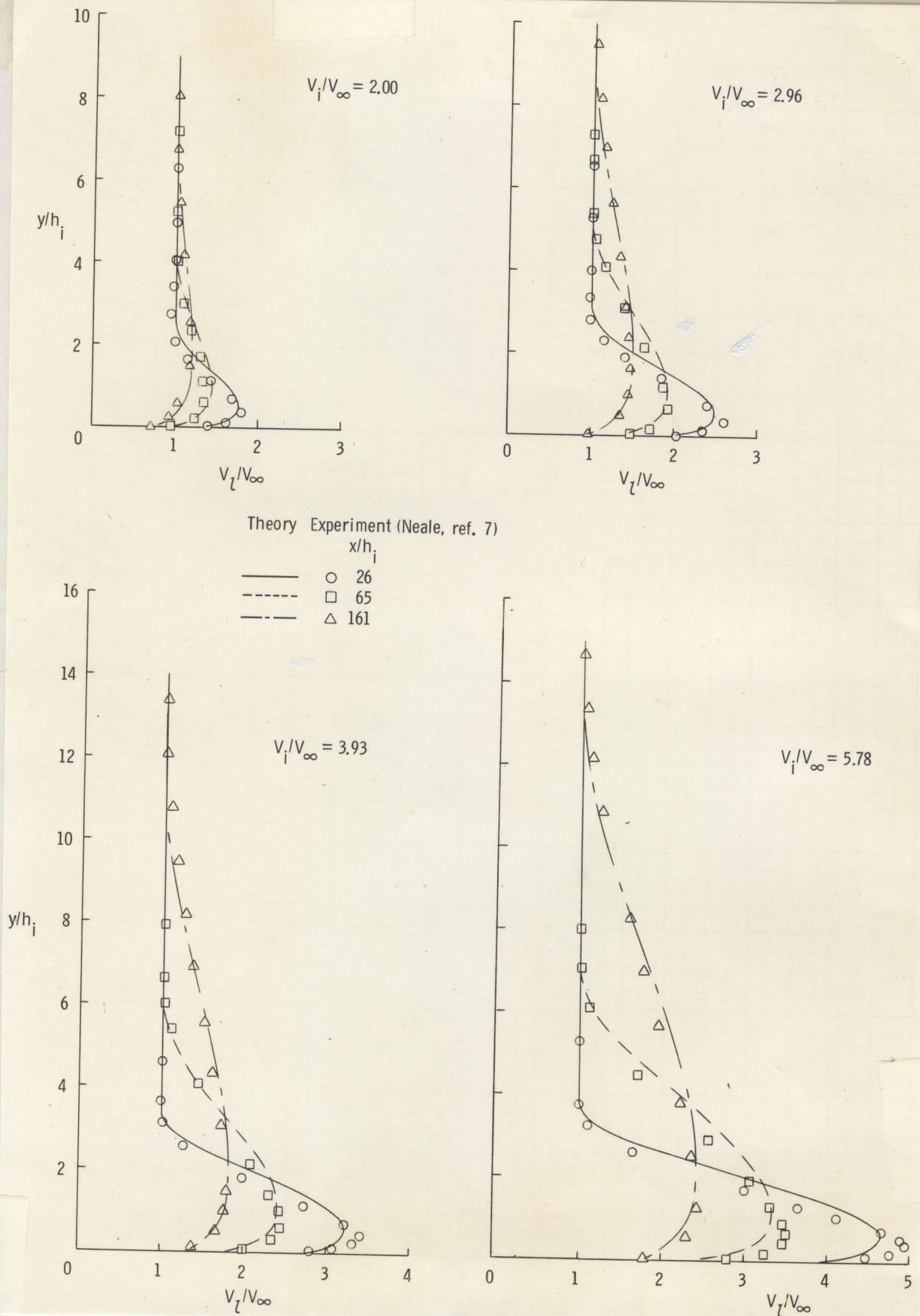
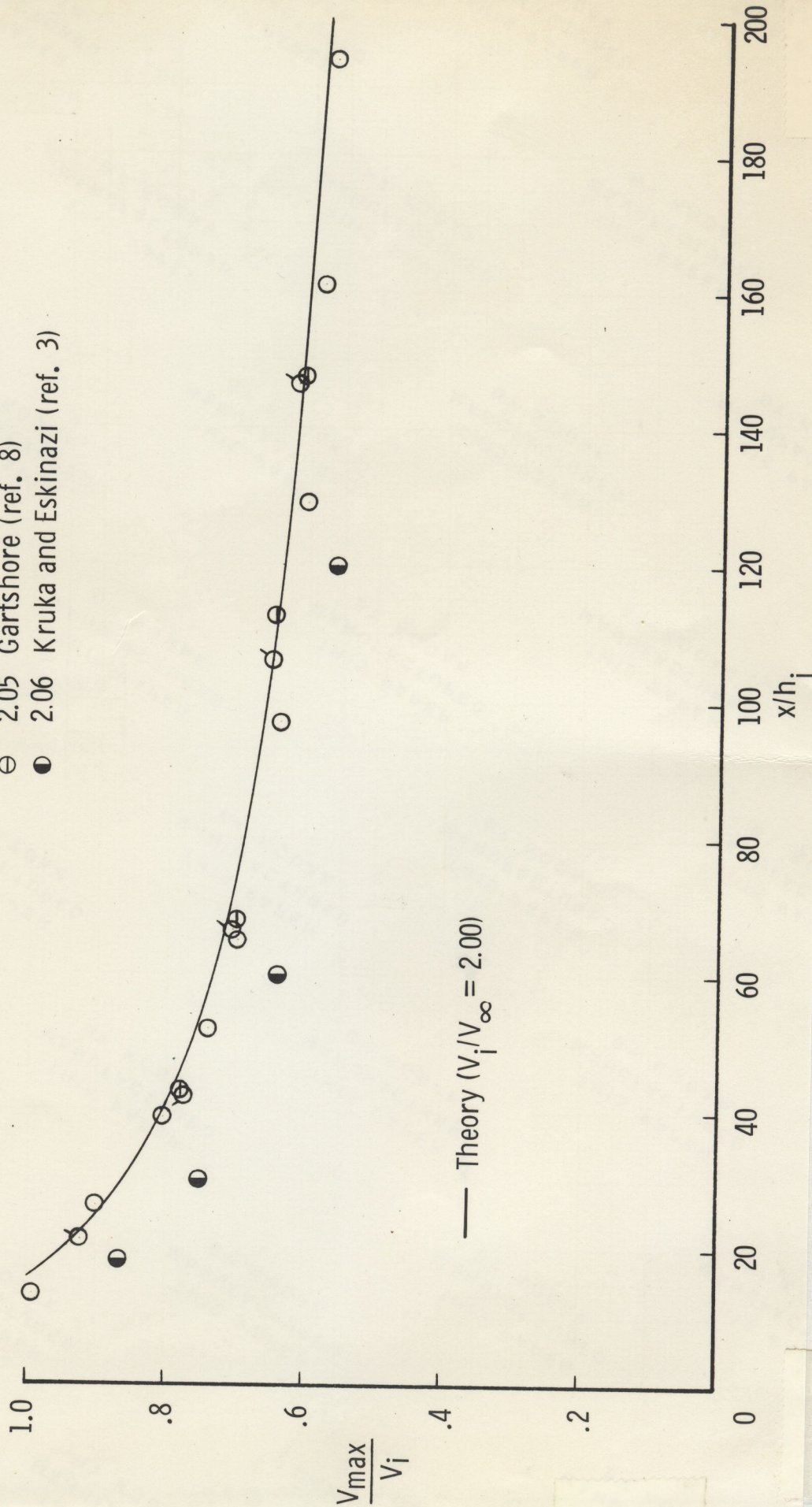


Figure 3.- Comparison of experimental and theoretical velocity profiles.

Experiment
 V_i/V_∞

- 2.00 Neale (ref. 7)
- ◊ 2.05 Gartshore and Newman (ref. 6)
- ⊖ 2.05 Gartshore (ref. 8)
- 2.06 Kruka and Eskinazi (ref. 3)



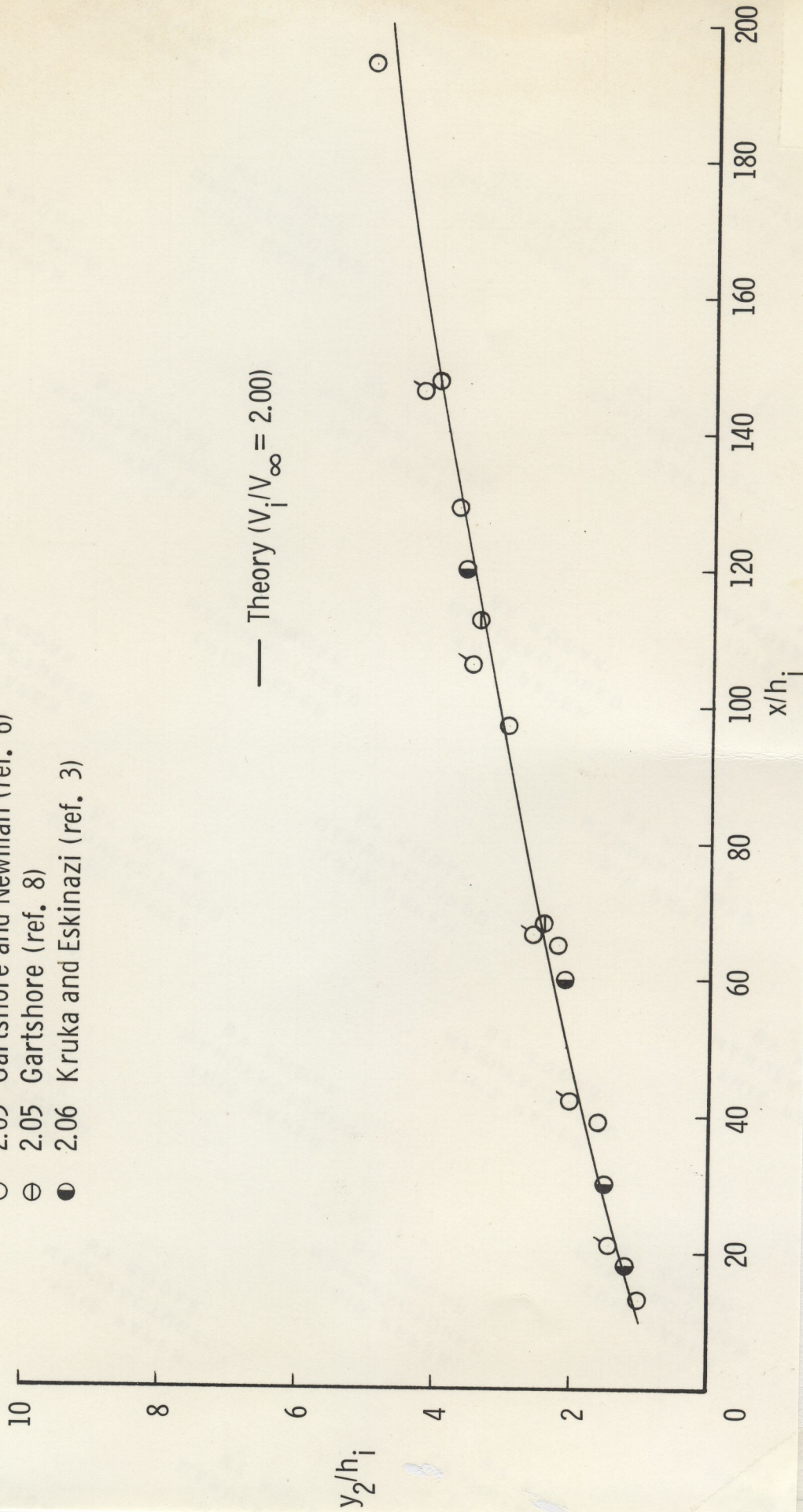
(a) Velocity decay.

Figure 4.- Comparison of experimental and theoretical wall-jet development for $V_i/V_\infty \approx 2$.

Experiment
 V_i/V_∞

- 2.00 Neale (ref. 7)
- ◊ 2.05 Gartshore and Newman (ref. 6)
- ⊖ 2.05 Gartshore (ref. 8)
- 2.06 Kruka and Eskinazi (ref. 3)

— Theory ($V_i/V_\infty = 2.00$)

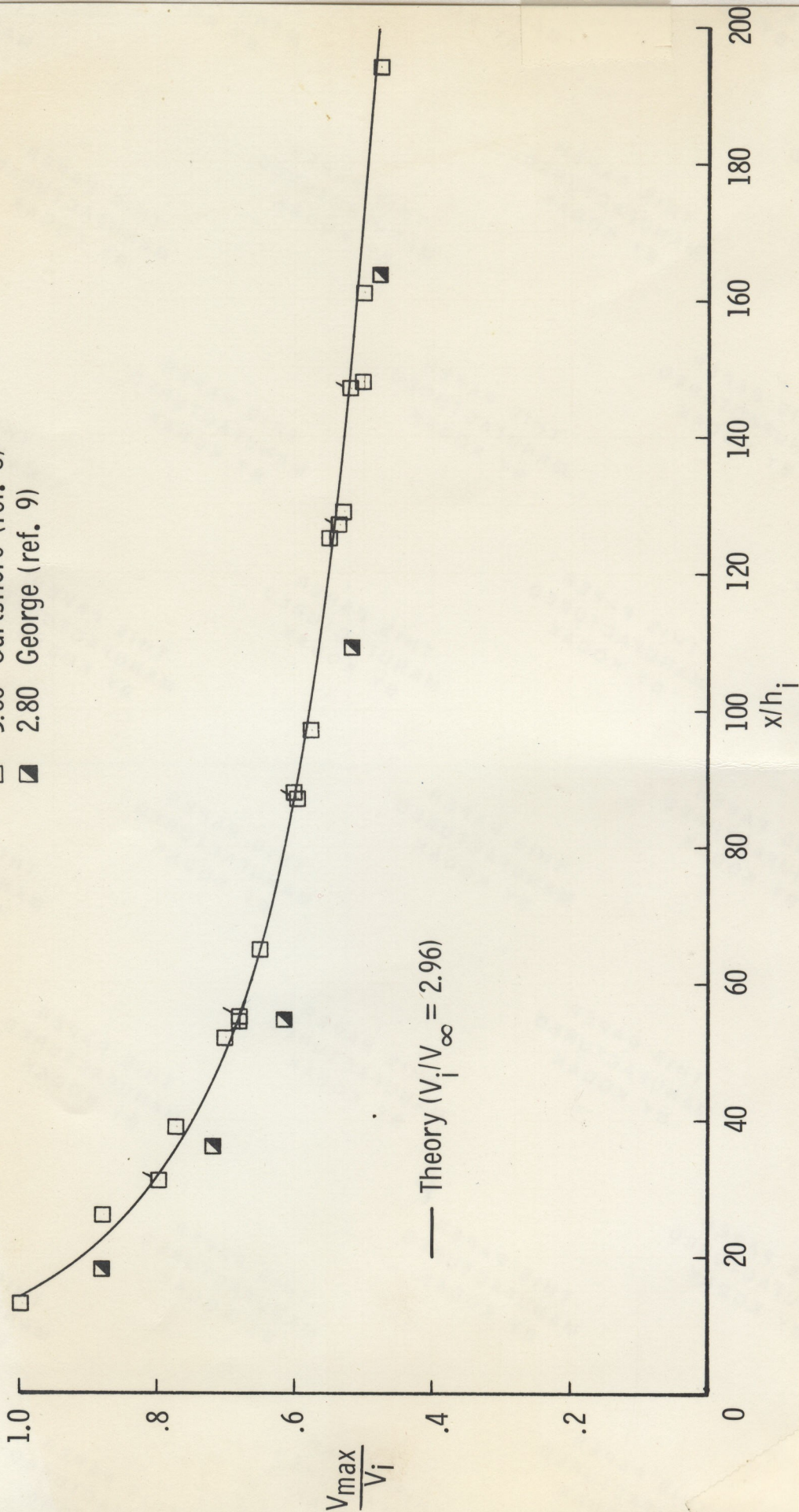


(b) Jet growth.

Figure 4. - Concluded.

Experiment
 V_i/V_∞

- Neale (ref. 7)
- ◻ Gartshore and Newman (ref. 6)
- ◻ Gartshore (ref. 8)
- ◼ George (ref. 9)



(a) Velocity decay.

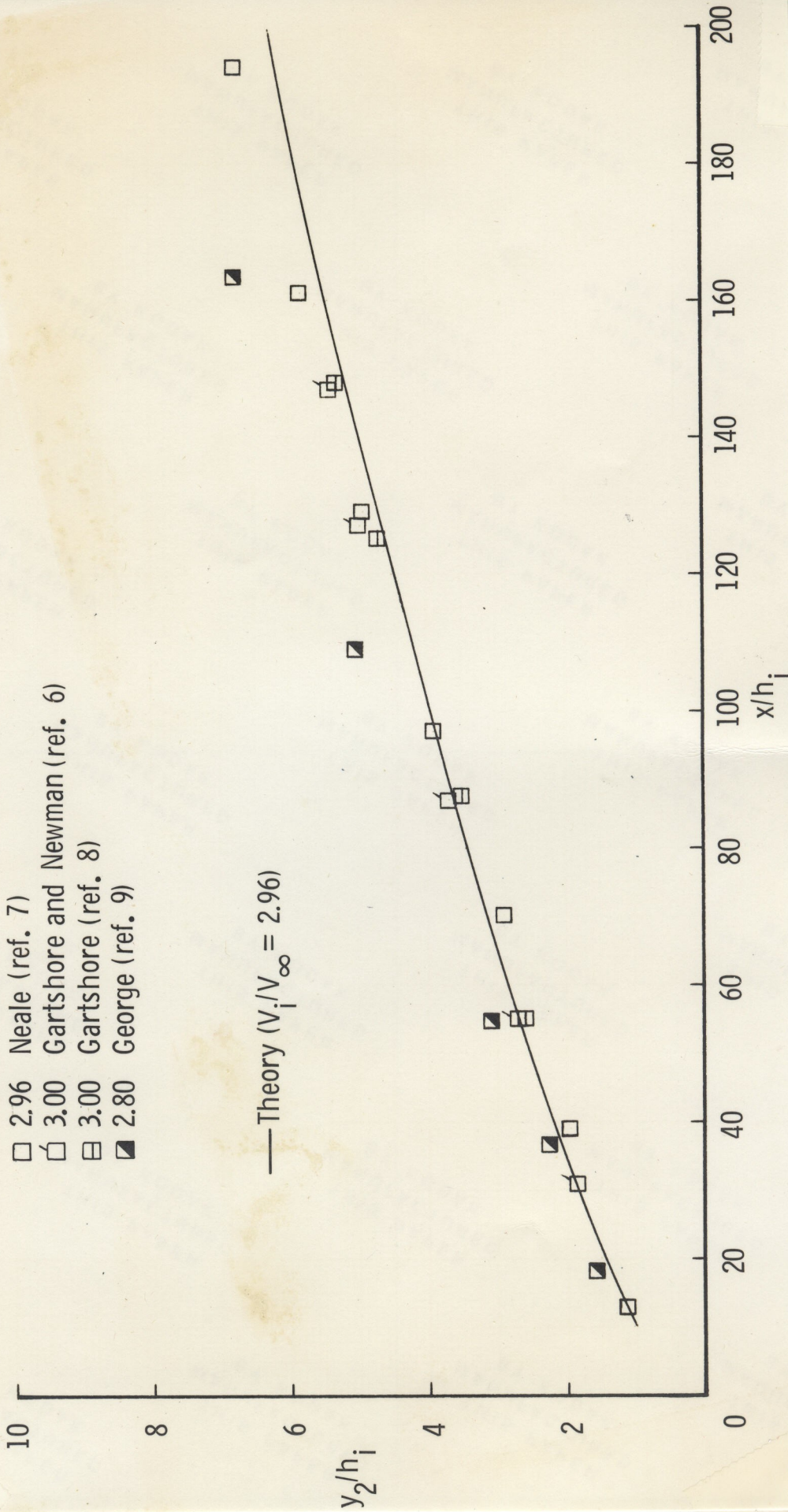
Figure 5.- Comparison of experimental and theoretical wall-jet development for $\frac{V_i}{V_\infty} \approx 3$.

Experiment

V_i/V_∞

- 2.96 Neale (ref. 7)
- ◻ 3.00 Gartshore and Newman (ref. 6)
- ◻ 3.00 Gartshore (ref. 8)
- ◼ 2.80 George (ref. 9)

— Theory ($V_i/V_\infty = 2.96$)



(b) Jet growth.

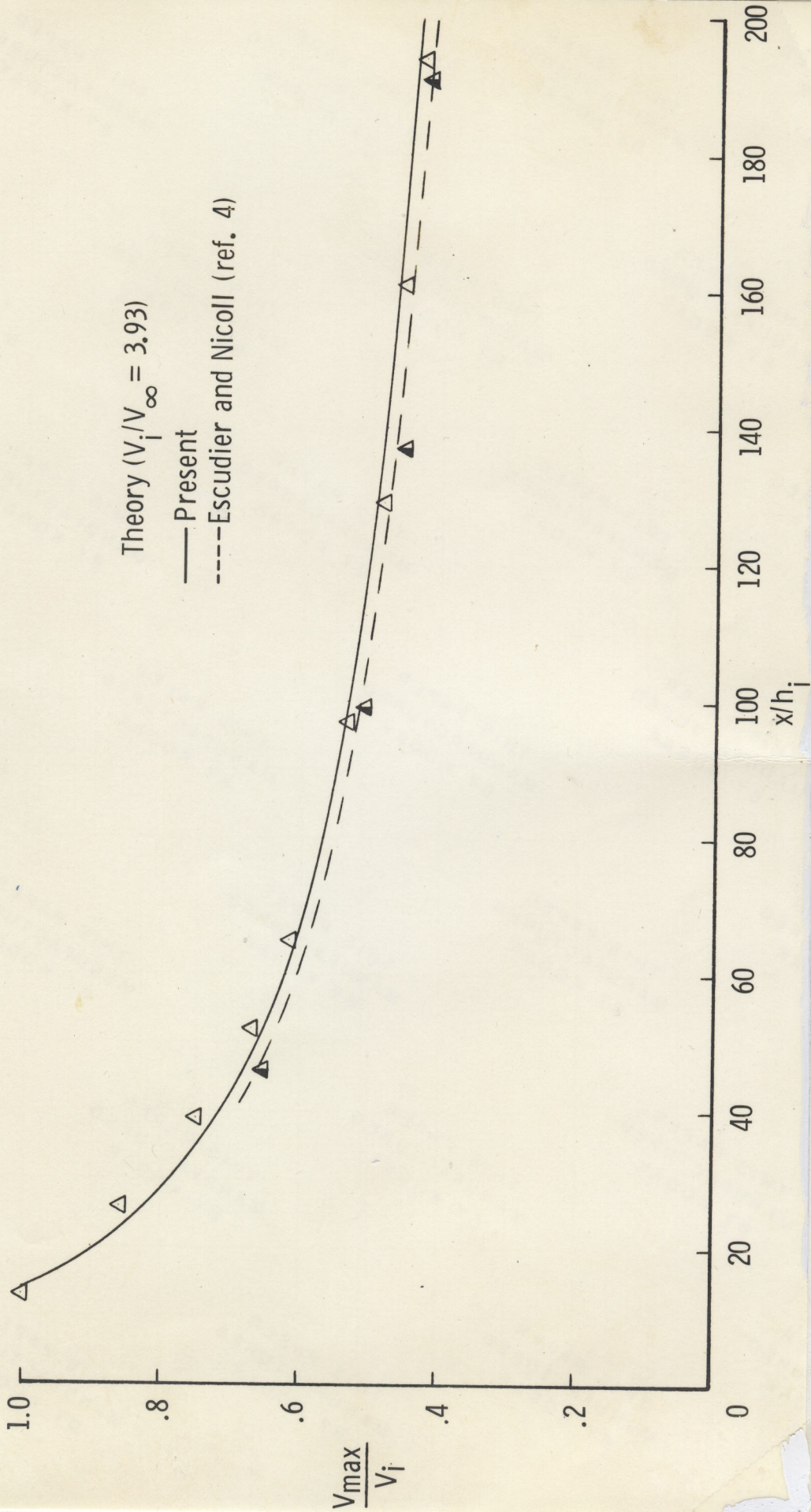
Figure 5.- Concluded.

Experiment
 V_i/V_∞

- ▲ 3.80 Kruka and Eskinazi (ref. 3)
- △ 3.93 Neale (ref. 7)

Theory ($V_i/V_\infty = 3.93$)

- Present
- - - Escudier and Nicoll (ref. 4)



(a) Velocity decay.

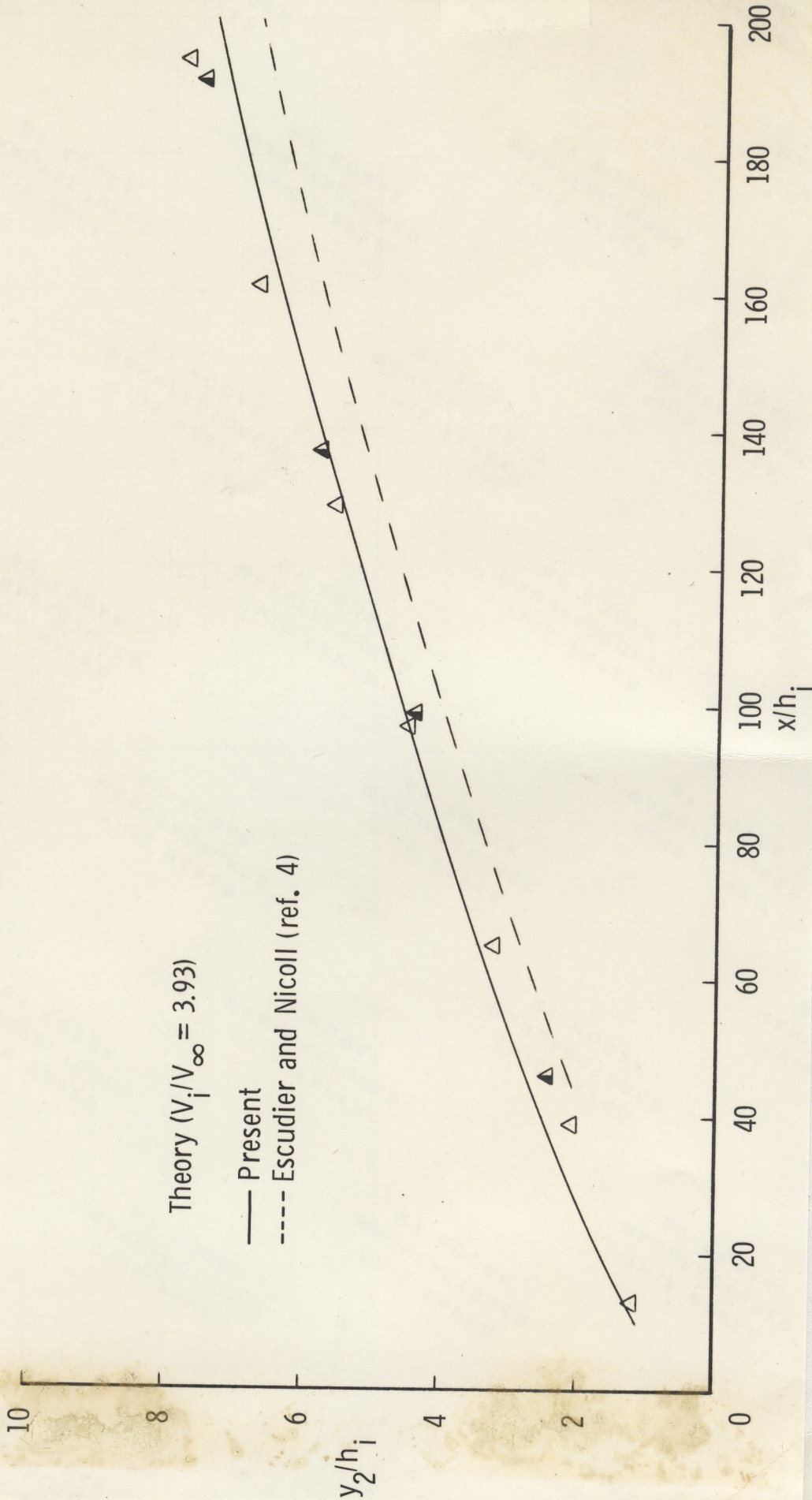
Figure 6.- Comparison of experimental and theoretical wall-jet development for $V_i/V_\infty \approx 4$.

Experiment
 V_i/V_∞

- ▲ 3.80 Kruka and Eskinazi (ref. 3)
- △ 3.93 Neale (ref. 7)

Theory ($V_i/V_\infty = 3.93$)

- Present
- - - - Escudier and Nicoll (ref. 4)



(b) Jet growth.

Figure 6. - Concluded.

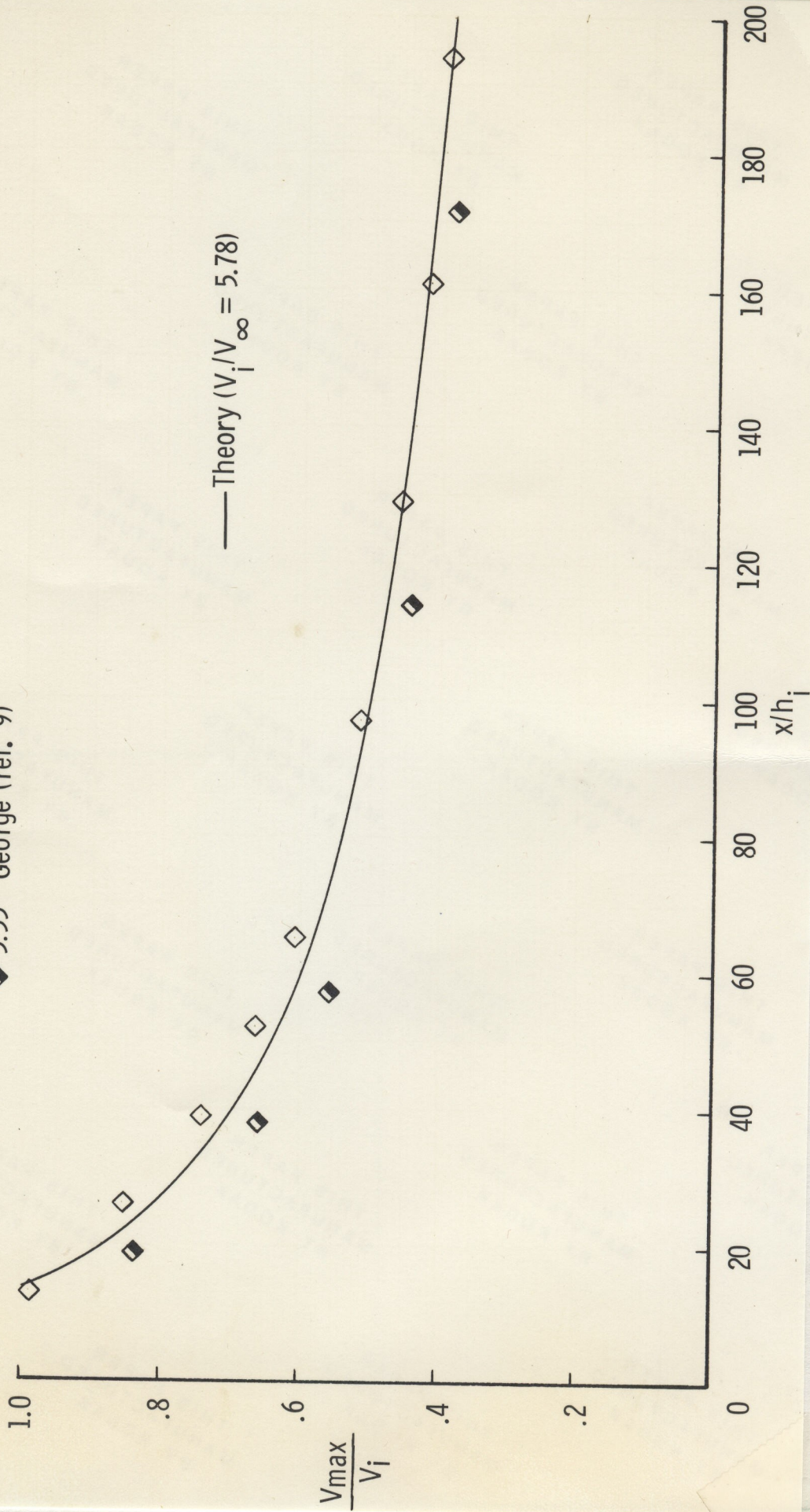
Experiment

V_i/V_∞

◇ 5.78 Neale (ref. 7)

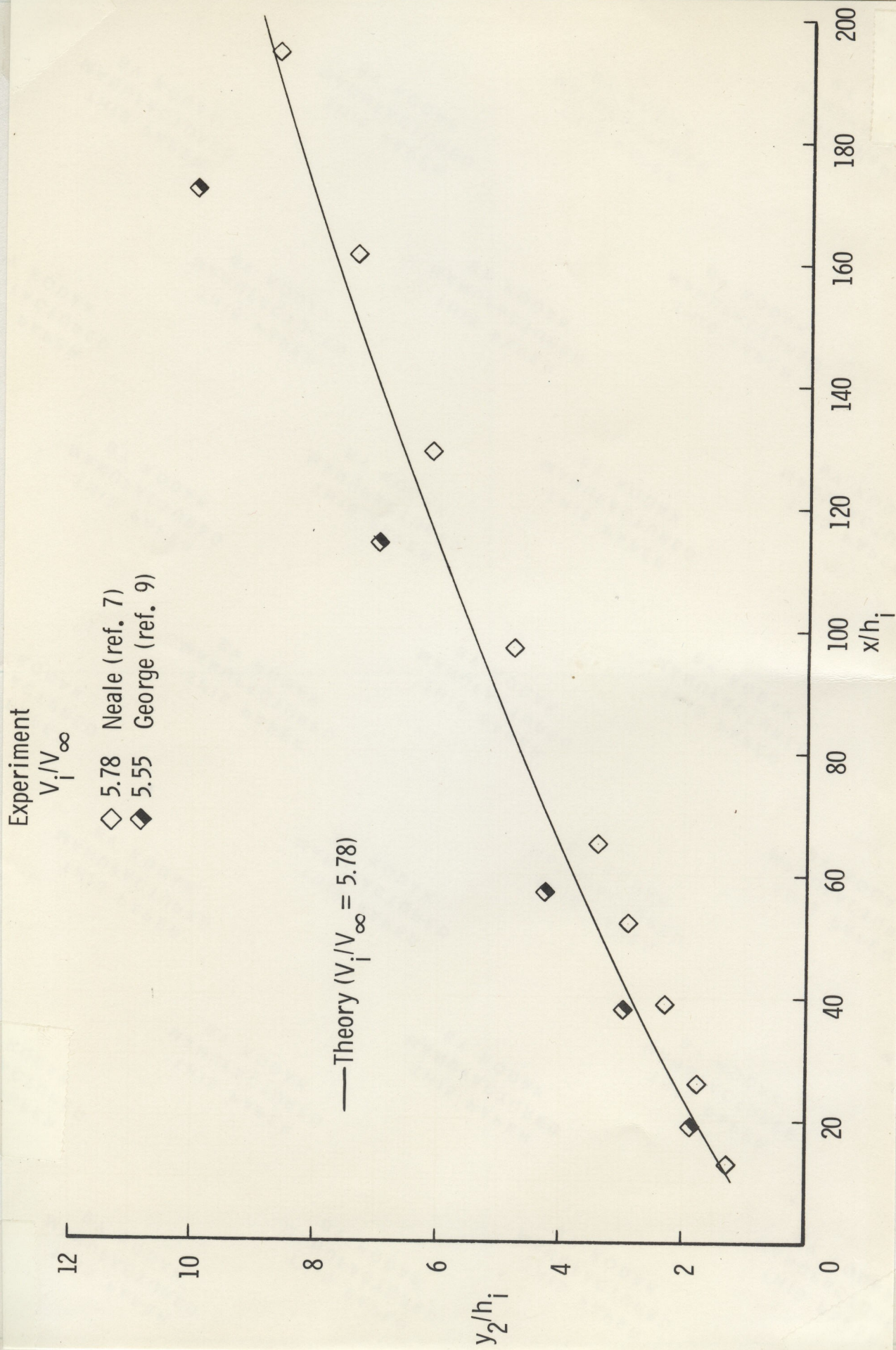
◆ 5.55 George (ref. 9)

— Theory ($V_i/V_\infty = 5.78$)



(a) Velocity decay.

Figure 7.- Comparison of experimental and theoretical wall-jet development for $V_i/V_\infty \approx 6$.



(b) Jet growth.
Figure 7.- Concluded.

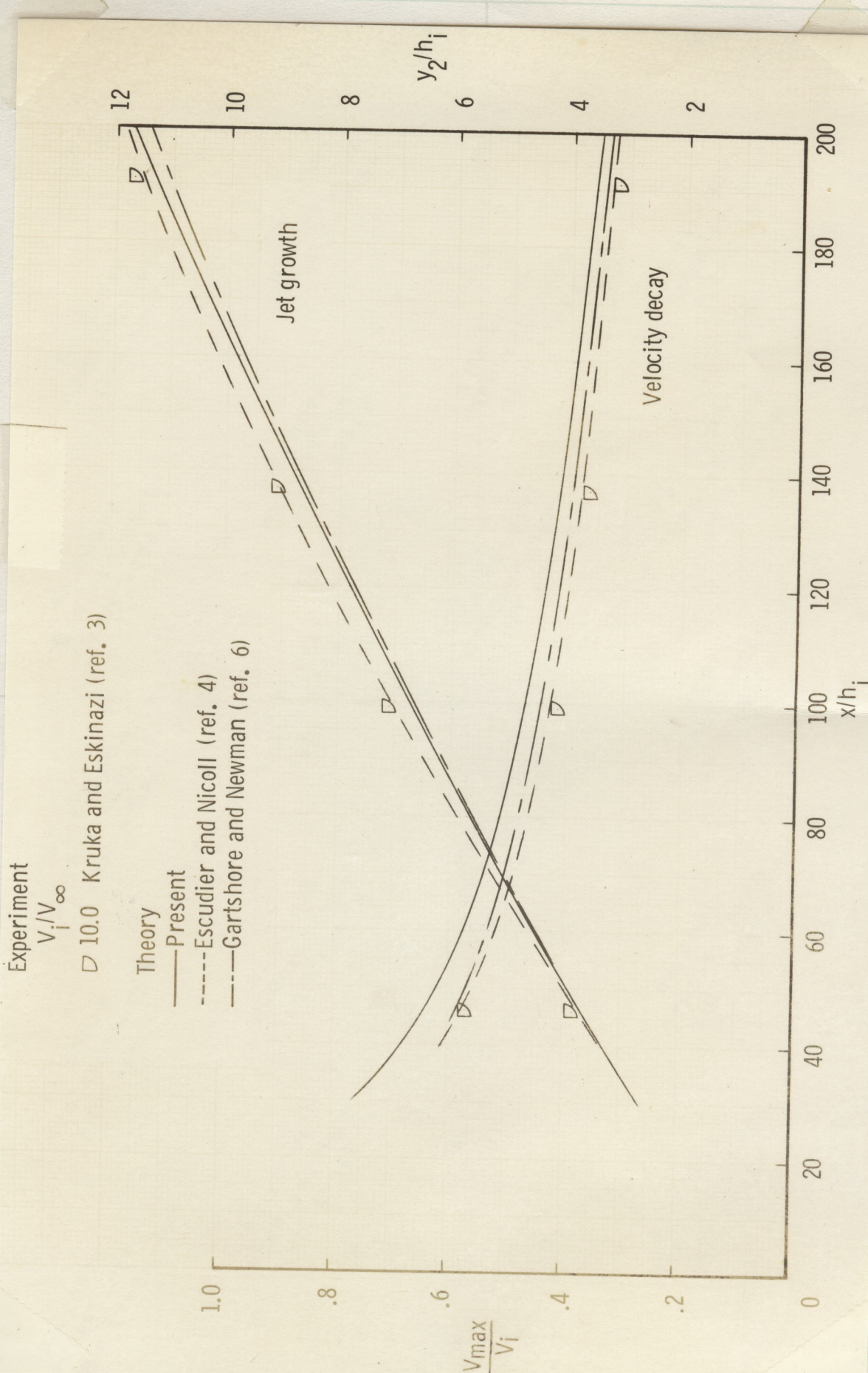


Figure 8.- Comparison of experimental and theoretical wall-jet development for $V_i/V_\infty \approx 10$.

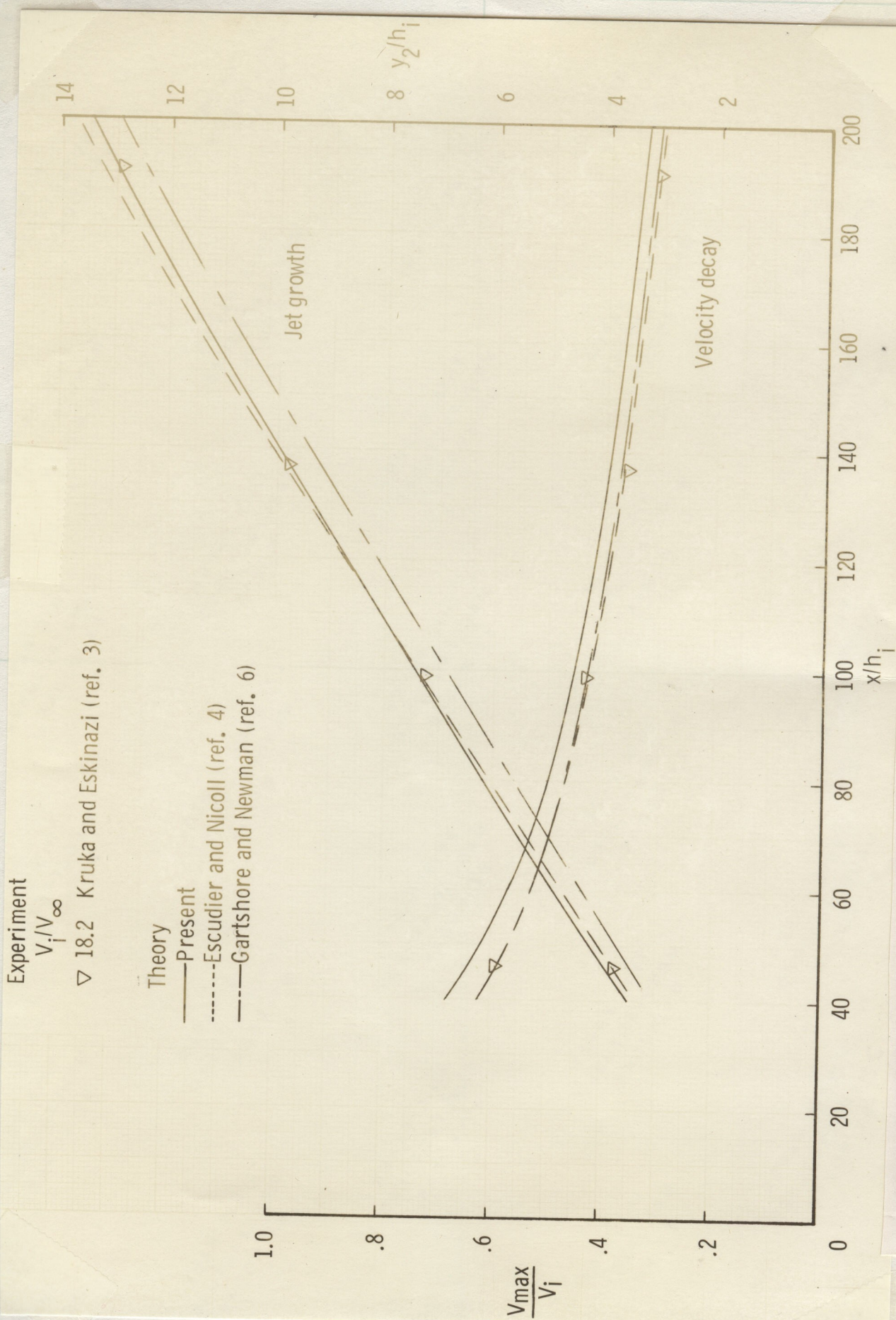


Figure 9.- Comparison of experimental and theoretical wall-jet development for $V_i/V_\infty \approx 18$.

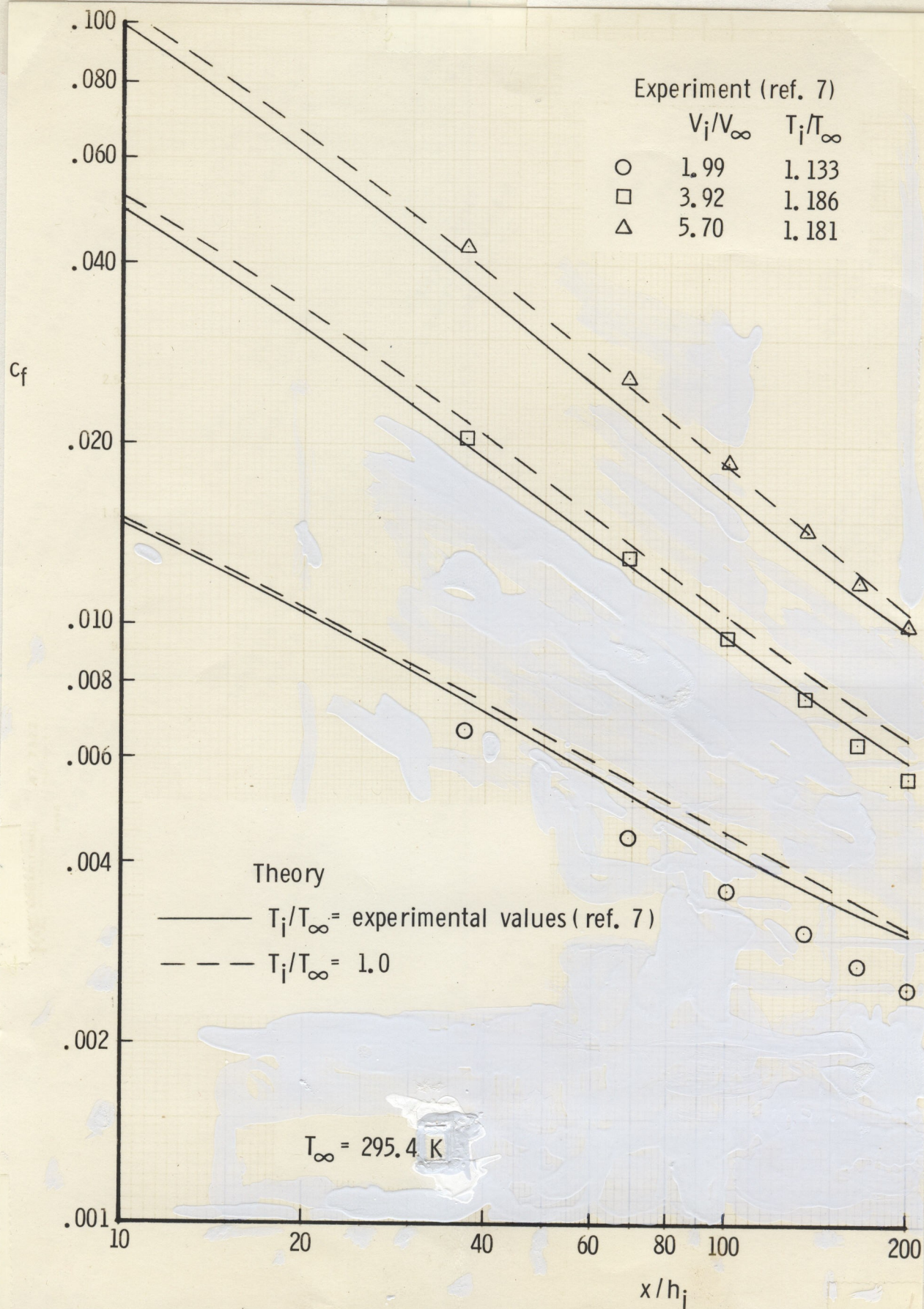


Figure 10.- Comparison of experimental and theoretical skin-friction coefficients.

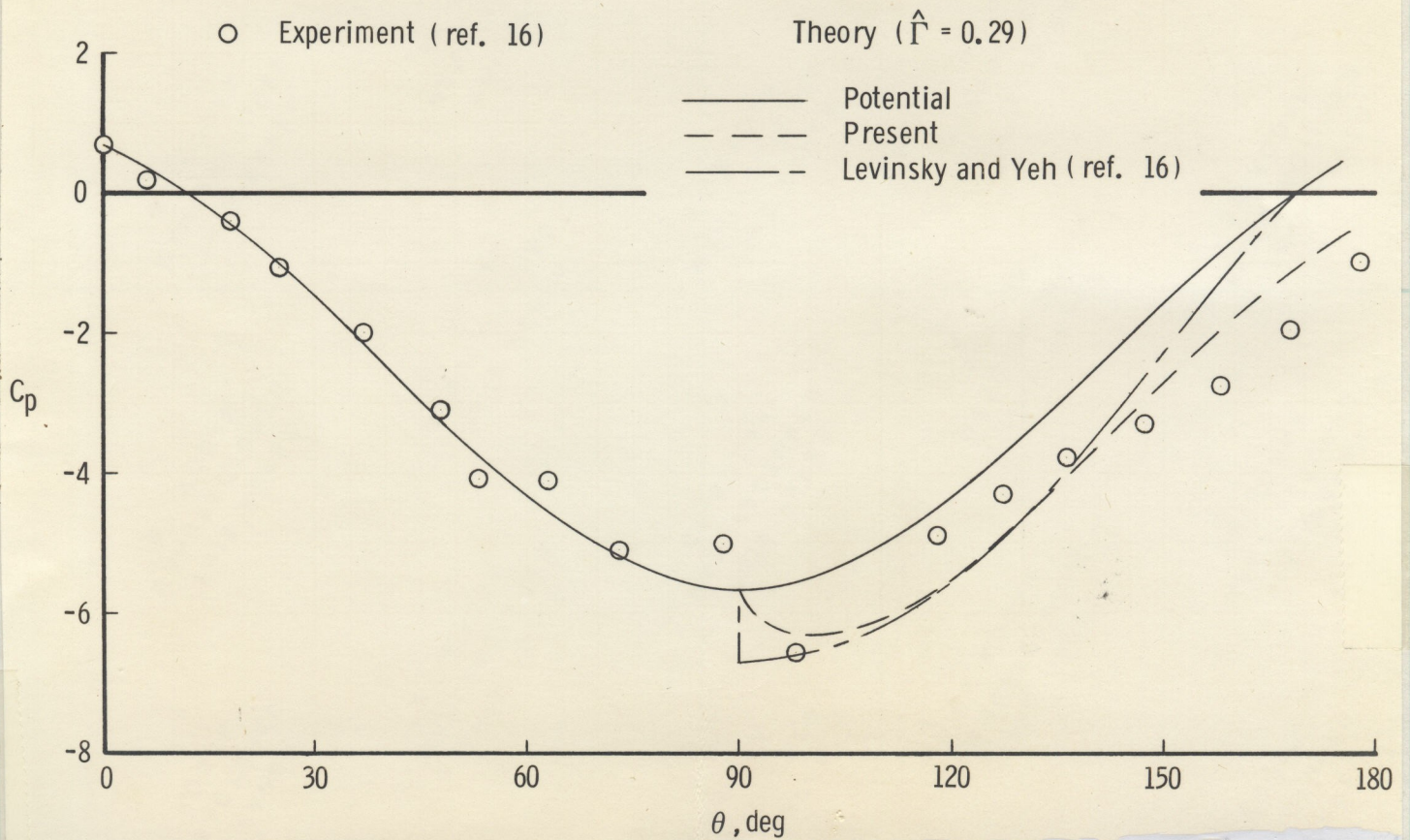
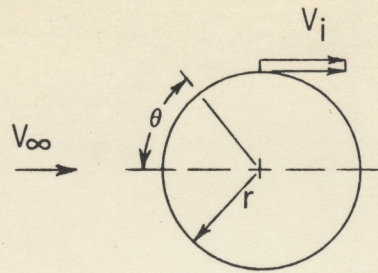


Figure 11.- Experimental and theoretical pressure distributions on circular cylinder with blowing at $\theta = 90^\circ$. $\frac{V_i}{V_\infty} = 7.24$; $\frac{h_i}{r} = 0.0057$.